J. Fluid Mech. (1995), *vol.* 292, *pp.* 205–227

An experimental investigation of Taylor vortex flow between conical cylinders

By MANFRED WIMMER

Institut für Strömungslehre und Strömungsmaschinen, Universität (TH) Karlsruhe, Germany

(Received 29 March 1994 and in revised form 3 January 1995)

Viscous flows and instabilities between conical cylinders are described which result from rotating an inner cone while the outer one is at rest. Both cones have the same apex angle resulting in a constant width of the gap between the bodies. The laminar basic flow is tree-dimensional. Owing to different centrifugal forces on the cone's surface one obtains regions of sub- and supercritical flows in the annulus. The Taylor vortices generated can be steady or unsteady, so that toroidal or helical vortices travel through the closed system, depending on different initial and boundary conditions. Furthermore, combinations of steady toroidal and unsteady helical vortices are possible. The influence of the governing parameters, like acceleration rate, gap width, end plates and so on is discussed. A comparison with available calculations is made.

1. Introduction

The flow between concentric rotating cylinders, as described by Taylor (1923), is one of the most investigated problems of the motion near rotating bodies. Viscous flows near and between rotating circular cylinders have been of interest to many scientists over the last 300 years, as discussed in Donnelly's (1992) essay. However, the pioneering work in this field was done by Taylor (1923) who, seventy years ago, described theoretically and proved experimentally the existence of toroidal vortices in the gap between two rotating cylinders. Since then, this kind of flow has been the subject of investigation by research workers of many disciplines, so that an abundance of results on circular Taylor–Couette flow is available.

Taylor vortices may also appear in geometries other than right circular cylinders, for instance between rotating spheres, previously described by Wimmer (1976). Another simple variation of the classical Taylor–Couette geometry is the flow between coaxially rotating cones, to be described in the following.

In contrast to circular cylinders, a three-dimensional basic flow is established between rotating conical cylinders. For infinitely long rotating circular cylinders, the centrifugal forces are uniform over the whole axial length, generating a rotationally symmetric one-dimensional basic flow, the circular Couette flow. In changing from circular to conical cylinders, the radius changes linearly resulting in a linear change of the centrifugal forces. Now, adjacent points on the cone's surface are no longer at the same conditions, causing an imbalance of the centrifugal forces in the annulus that drives the three-dimensional basic flow mentioned above.

The axially different centrifugal forces and the three-dimensional basic flow have significant consequences for the onset, occurrence and behaviour of the Taylor vortices generated in this case. Therefore, the flow between conical surfaces provides effects which contribute to a better understanding of the development of the vortices. Besides

giving insight into fundamental fluid mechanics, this kind of flow offers the possibility of a direct technical application. Hence, there is considerable value in its study.

2. Test arrangements and notation

The experimental investigations were conducted with an inner cone rotating and an outer one at rest. Figure 1 shows a sketch of the experimental set-up. The inner and the outer cones have the same apex angle of $\Phi = 16.03°$ giving a constant width of the gap for coaxially rotating bodies. The base radius of the outer cone R_{2max} is fixed at 50 mm, while that of the inner cone R_{1max} varies between 45 and 40 mm. Thus, gap sizes of $s = R_2 - R_1$ between 5 and 10 mm have been investigated. The length of the fluid column is fixed at $l = 125$ mm. These dimensions result in radius ratios $\eta = R_1/R_2$ between 0.9 and 0.8, and aspect ratios $\Gamma = l/s$ from 25 to 12.5.

The rotating inner cone is made of an aluminium alloy, while the outer cone is machined from transparent Plexiglas, so that the flow can be observed visually. Silicone oils are used as working fluids. The flow is made visible by a small amount of aluminium flakes. It was found that, for flakes with a typical dimension of 30 μm, a concentration of less than 2 g l^{-1} produces good signals when visualization with reflected light was used. For visualization with the light sheet technique a considerably smaller amount of aluminium flakes is necessary. With this technique we obtain information about the flow structure and development in a vertical cross-section of the annulus. The sketches presented are based on these observations. The above-mentioned aluminium concentration does not influence the viscosity of the silicone oils used or the flow field. The inner cone is driven by a variable-speed electric motor. The speed of rotation is controlled by photo-optics and the temperature of the fluid by thermistors with an accuracy better than 0.1 °C. By using silicone oils of various kinematic viscosities ν from 5 to 200 cS and by varying the speed of rotation, a wide range of Reynolds numbers could be covered.

From experience and preliminary experiments (cf. Wimmer 1983) it was known that disturbances start preferentially at the cone's apex and travel through the gap, disturbing the flow. In the present investigation, the apex has been removed and thus there is an arrangement of two truncated cones as displayed in figure 1. Such a configuration also has the advantage of being suspended at either end, avoiding unwanted vibrations. The gap between the cones is axially limited by end plates. Owing to manufacturing constraints the end plate at the bottom is stationary. The ring at the top is interchangeable, so that stationary and rotating end plates can be chosen. Depending on the rings' size, the width of the gap can be bridged completely or only partially, as illustrated in figure 1. The different boundary conditions will have an influence on the flow configurations occurring, so that, together with different initial conditions, a wide variety of flow patterns can be generated.

To specify the problem, a cylindrical coordinate system is used and is specified in figure 1. The dimensionless quantities characterizing the flow are: the Reynolds number $Re = R_{1max}^2\,\omega/\nu$, the Taylor number $T = R_{1max}\,s^3\omega^2/\nu^2$ or, in another form, $Ta = R_{1max}\,s\,\omega/\nu\,(s/R_{1max})^{1/2}$, with the relation $Ta = T^{1/2}$. Here ω denotes the angular velocity and ν the kinematic viscosity. These different characteristic numbers are used for comparison with flow problems in other geometries.

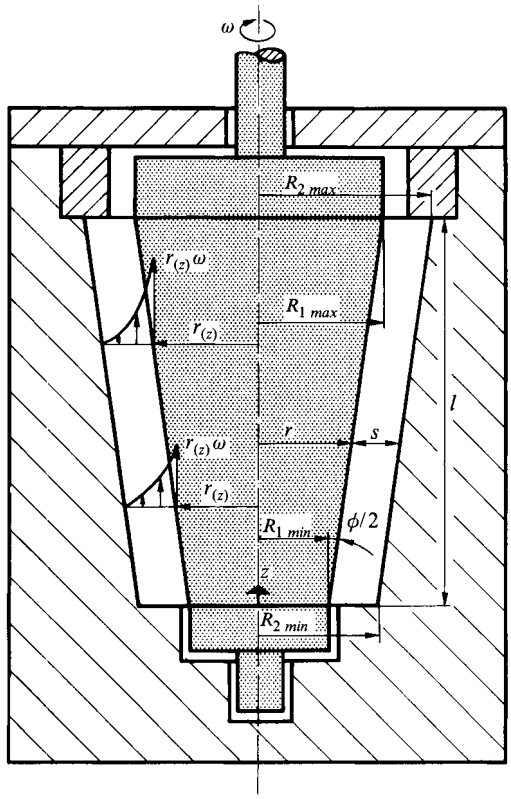

FIGURE 1. Experimental apparatus (dotted, aluminium; hatched, Plexiglas), notation and velocity profiles (turned through 90°).

3. Basic flow

The undisturbed laminar basic flow between rotating cones is already fully three-dimensional, driven by the previously mentioned imbalance of centrifugal forces in the annulus. At the walls, the non-slip conditions apply. As a consequence, there is, on the inner rotating cone, a circumferential velocity $r_{(z)}\,\omega$, depending on the z-coordinate, while on the outer stationary cone, its value is always zero, as shown in figure 1. Hence, the circumferential velocity of the fluid in the annulus decreases with increasing radial and decreasing axial coordinates. This results in a negative rate of change of centrifugal forces in the r-direction and a positive change in the z-direction. The fluid is, therefore, deflected outwards at the largest radius, moves down in spirals to the smallest radius in the vicinity of the stationary shell and returns to the largest radius near the rotating cone, also in spiral form. The spirals form a closed flow. The meridional component of the three-dimensional flow is a large loop between the conical surfaces, as displayed in figure 2.

The meridional velocity component crucially influences the generation of the vortices and should be examined very carefully. The meridional flow depends on the angular velocity ω and on the apex angle Φ, causing the three-dimensionality. Furthermore, the meridional velocity is not uniform over the axial length, despite the constant gap width. The horizontal cross-section $A = (r_2^2 - r_1^2)\,\pi$ decreases from base to apex. Hence, owing to continuity, the meridional velocity will change correspondingly. There emerges, therefore, another dependence of the meridional velocity on the axial coordinate.

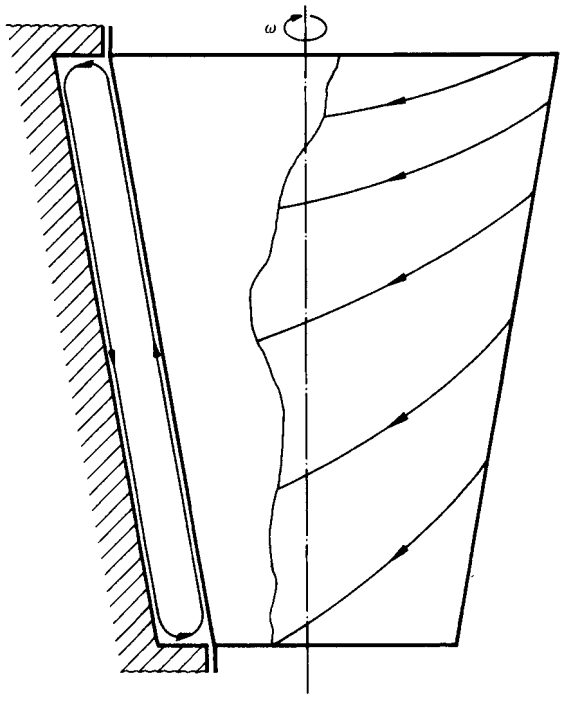

FIGURE 2. Three-dimensional basic flow.

In addition, the meridional velocity is also affected by the size of the gap. Owing to the non-slip condition on both walls (figure 1) there is a steeper gradient of the azimuthal velocity for smaller gap sizes than for larger. This fact produces different gradients of the driving forces, resulting in different meridional velocities. The vigour of the meridional velocity and hence its effect on the vortex cells to be generated depends upon: (i) the angular velocity ω, (ii) the apex angle Φ, (iii) the axial coordinate z, and (iv) the width of the gap s.

4. Occurrence and behaviour of Taylor vortices

In order to show the fundamental behaviour of the vortices, some parameters, for example apex angle Φ and gap width s, will be kept constant. A large gap size of $s =$ 10 mm is chosen, which permits the phenomena that occur to be demonstrated very clearly and provides clear photographs. In this case, the annulus is bounded by two stationary end plates bridging the gap completely.

Upon increasing the angular velocity of the inner cone, the centrifugal forces will progressively dominate the viscous forces. Disturbances of the basic flow then generate regular closed vortex cells, known as Taylor vortices, if the critical value of the Taylor number $T = rs^3\omega^2/\nu^2$ has been exceeded.

For a constant width of the gap, Taylor vortices will occur initially in the upper part of the annulus, where the centrifugal forces are largest. This happens such that, at the largest radius near the stationary end plate, a single vortex is generated. This single vortex, together with the rest of the basic flow, forms a pair of vortices, as illustrated in figure 3. The vortical flow does not start with a pair of Taylor vortices in addition to the rest of the basic flow, as might be assumed. The top-most vortex would then be forced to have a sense of rotation which is directed outwards at the stationary end

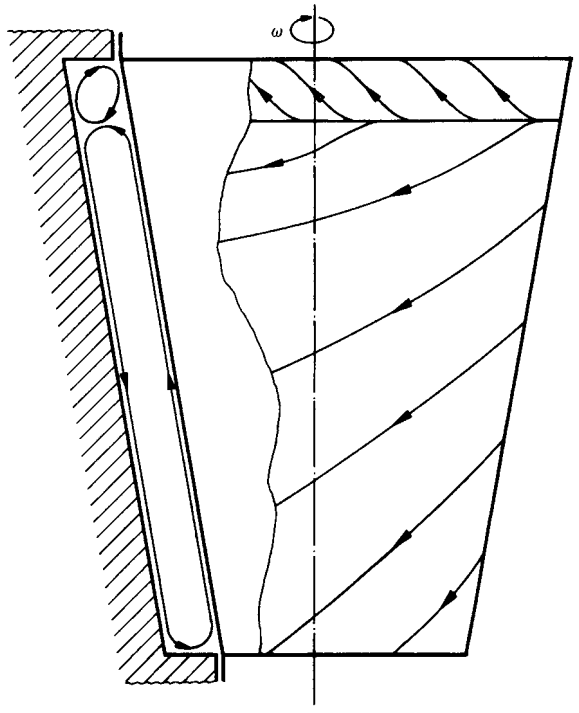

FIGURE 3. Location and sense of rotation of the first vortex that occurs.

plate. However, there is always a deceleration of the circumferential velocity due to the non-slip condition. The deceleration reduces the centrifugal forces and causes, because of constant pressure forces, a radial inward flow at the stationary end plate. The rest of the basic flow always maintains its original sense of rotation and determines the circulation of the initially still weak vortex at the horizontal top boundary. Hence, for the present configuration, the sense of rotation of both parts of the flow in the gap match where they meet. There is no opportunity for the formation of another vortex! Thus, the present arrangement is the only possible configuration, as was found during the experiments.

With a further increase of the angular velocity, another pair of vortices is produced, which separates from the upper part of the basic flow. In succession, more vortices are added in the direction towards the smaller radius. The vortex cells travel upwards to the larger radius, their upward motion being caused by the imposed meridional swirl, which dominates over the still weak vortices.

Since the centrifugal forces are a function of the axial coordinate, a part of the annulus is already supercritical while the other part is still subcritical. As a consequence, different types of flow, both stable and unstable, may exist simultaneously side by side, as is also the case between rotating spheres (Wimmer 1976). Figure 4 illustrates this phenomenon.

On increasing the angular velocity, more vortex pairs are generated until the whole gap is finally filled with vortices. At first, they are still travelling upwards. This happens in such a way that the top-most clockwise rotating vortex at the stationary end plate always remains, while the next three cells are compressed. In particular, the next clockwise rotating cell, rotating against the meridional flow, is compressed to such an extent, that it vanishes. The two neighbouring vortices join together to form one large counterclockwise rotating cell, establishing, together with the top vortex, a new pair.

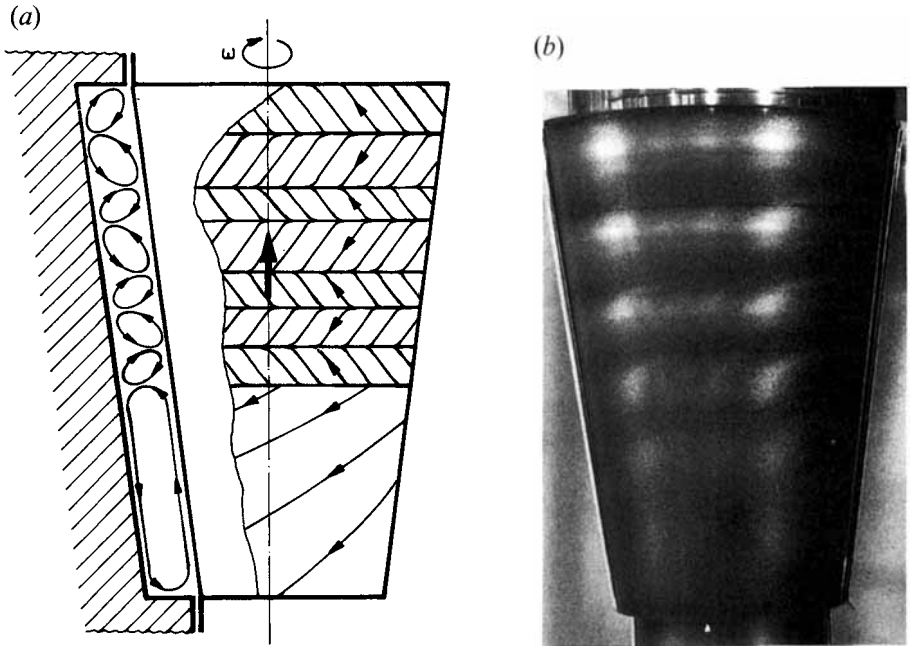

FIGURE 4. Sub- and supercritical regions in the annulus. (*a*) Streamlines, (*b*) photograph; $s = 10$ mm, $Re = 440$.

The adjacent pair follows, while at the bottom a new pair is generated. The whole procedure then starts anew and is periodic.

This behaviour was also found theoretically by Abboud (1988). His numerical calculations demonstrate the linear velocity of the upwards travelling vortices as well as their different size. He also proved theoretically the disappearance of the third vortex cell and the periodicity of the procedure. The time sequence of the development is shown in figure 5, which is based on Abboud's contribution. During the movement the vortices keep their form as closed toroidal cells, the axes of which point in the azimuthal direction. Hence, a pattern of toroidal vortices travels through a closed system.

The velocity of the upwards travelling vortices depends on the meridional velocity. This, once again, is a function of the angular velocity ω, the apex angle Φ and the gap width s. We can assume therefore, that the travel velocity also depends on these parameters. Actually the assumption is valid for Φ and s, because the upward motion of the vortices increases with increasing apex angle and decreasing gap size. For the angular velocity an opposite effect is observed: the velocity of the upwards travelling vortices decreases with increasing angular velocity. It may be argued that this effect is caused by the locally different strength of the vortices and the meridional flow. The meridional flow becomes stronger with increasing angular velocity, as do the centrifugal forces. This results in more vigorous vortices, especially at the larger radius where the meridional flow is relatively weak. Consequently the vortices may become so vigorous that they can overcome the influence of the meridional flow. As a result, the speed of the upward motion slows down until a steady state is reached. Such a phenomenon is actually observed for larger gap sizes.

The velocity of the travelling vortices was measured between two fixed marks on the outer cone. This distance D between the marks can be determined with an accuracy of

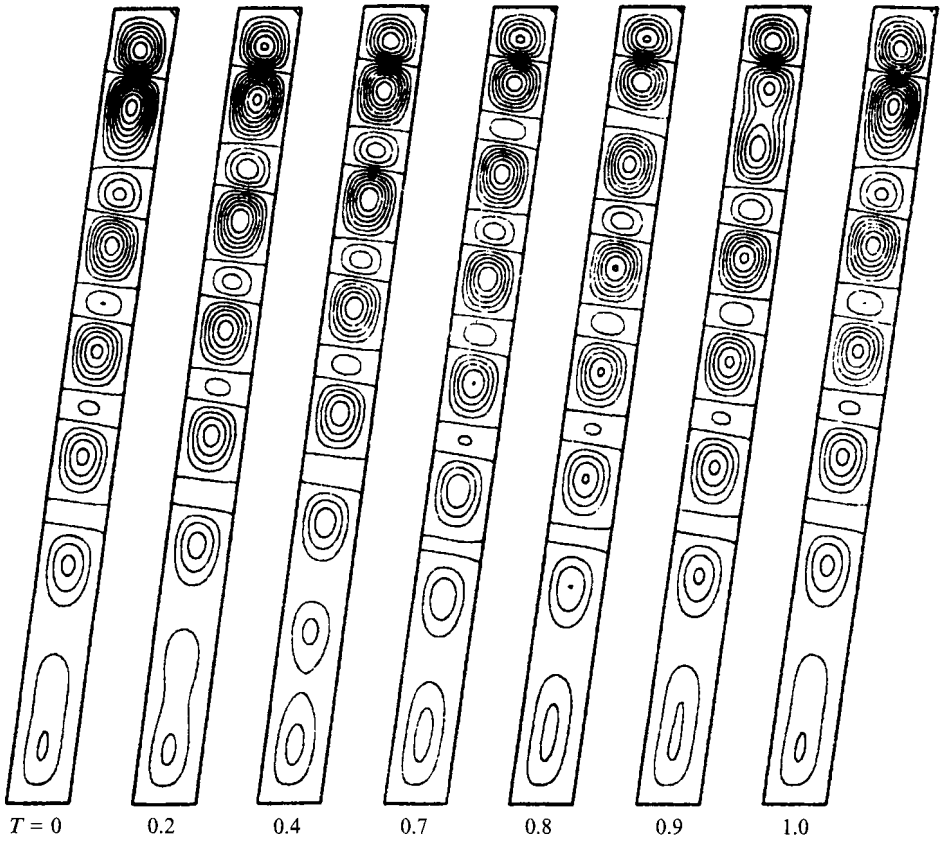

FIGURE 5. Calculated periodicity of the development of the vortices. One period $T = t/P_t$, where t is the actual time and P_t the time of one period.

better than 0.5 mm. The time t taken by a vortex to pass the distance between the two marks was measured by a stop watch with an accuracy of 0.1 s. An average value out of five different time measurements was used to calculate the velocity $c = D/t$ of the upwards travelling vortices. This results in an overall accuracy of 3%, except for the beginning of the motion where the annulus was not yet entirely filled with vortices. Figure 6 shows the travel velocity for a gap width of $s = 10$ mm. We see that the dimensionless velocity of the vortices decreases linearly with growing Reynolds number, i.e. with increasing centrifugal forces, until at about $Re = 930$, corresponding to $Ta = 117$, a steady state is reached.

If the basic flow dominates the vortex flow only slightly, then a shift of the entire vortex system occurs, as in the present case. Only then, when the established vortices are vigorous enough to mask the basic flow, does the shift stop and the influence of the basic flow is confined to a single vortex cell. In the present experiment, this fact is apparent in different extensions of adjacent vortex cells. If a vortex rotates in the direction of the meridional flow (in the following called a co-rotating vortex), it is stretched; if it rotates in the opposite direction (in the following called a contra-rotating vortex), it is compressed. Since Taylor vortices preferentially occur as counter-rotating tori, alternatively large and small vortex cells occur in the annulus between conical cylinders, as demonstrated in figure 7(*a*, *b*).

As mentioned above, the basic flow is directed radially outwards at the upper stationary end plate and inwards at the lower one. Normally, vortices adjacent to

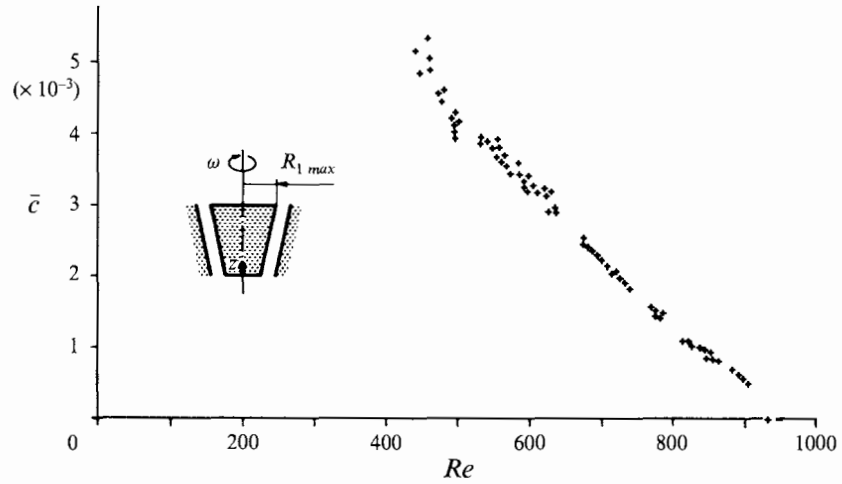

FIGURE 6. Vertical velocity $\bar{c} = c/R_{1max}\omega$ of travelling toroidal vortices; c is the actual measured velocity, $Re = R_{1max}^2\omega/\nu$, $s = 10$ mm.

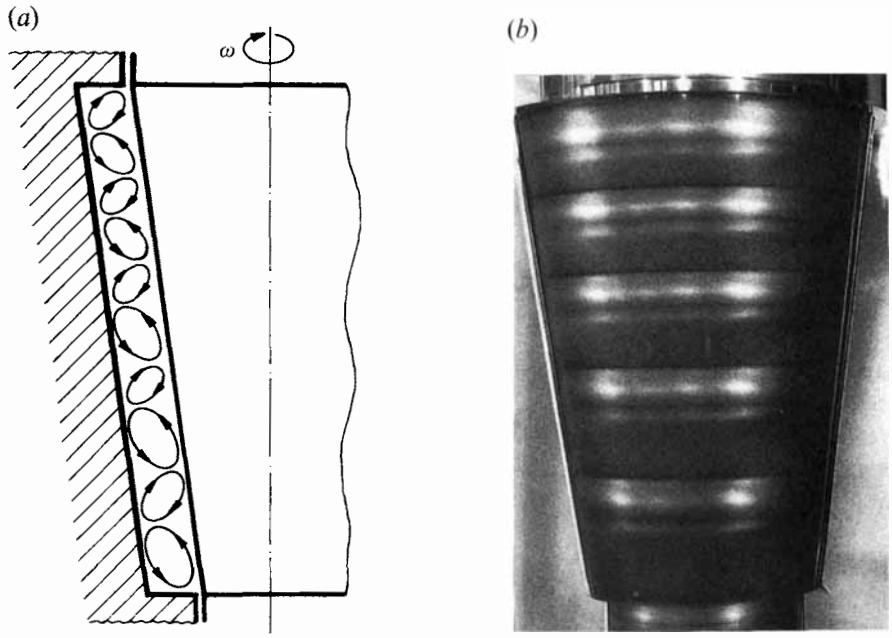

FIGURE 7. Cell size and arrangement for five vortex pairs. (*a*) Meridional streamlines, (*b*) Photograph; $s = 10$ mm, $Re = 1411$.

stationary end plates have an inward velocity component, as explained at the beginning of the section and reported for the case of Taylor vortices between circular cylinders by Burkhalter & Koschmieder (1973). Since Taylor vortices usually appear in pairs, an even number of vortices will be generated in the annulus with two stationary end plates. Consequently, one end vortex is forced to rotate opposite to the basic flow. In order to decide which of the vortices, that at the top or at the bottom, rotates opposite to the meridional flow, the interaction of the meridional and vortex flow must be clarified. At the largest radius the meridional flow is weakest, while at the smallest radius it is strongest. At the top the vortices are most vigorous while at the bottom they are

weakest. As a consequence, at the largest radius, where there is the weakest meridional flow and strongest vortex rotation, the top vortex will rotate opposite to the meridional flow. A steady state therefore results with an even number of vortices, having alternately large and small cells, as sketched in figure 7(*a*) and demonstrated by the photograph figure 7(*b*).

5. Non-uniqueness

5.1. *Final steady states*

The annulus is completely filled with vortices if supercritical conditions are established everywhere. For higher Reynolds numbers, the upward motion of the vortices stops and a steady pattern is established. The steady state is, however, not unique even with constant boundary conditions.

The existence of non-unique flow modes was reported by Coles (1965) and by Burkhalter & Koschmieder (1974) for the case of circular cylinders, and by Wimmer (1976) for concentric spheres. The different modes of flow, all existing at the same characteristic number, can be obtained either by a change from one mode to another, or by changing the initial conditions from the laminar basic flow. In the experiments, different rates of acceleration must then be applied to the inner rotating body. From experience it is known that the smaller an initial acceleration rate the more stable is the generated mode of flow; likewise, the higher the rate of acceleration the higher the number of generated vortex cells.

The flow configurations and arrangements discussed so far all correspond to the mode of flow which is established for the smallest acceleration rate, e.g. a quasi-steady acceleration, for which five pairs of vortices are obtained in this annulus, as illustrated in figure 7(*b*). For higher rates of initial acceleration, six or seven pairs of vortices may occur with an unchanged geometry but with correspondingly smaller wavelengths of the cells. These modes can be seen in figure 8(*a*, *b*). For the case of rotating circular cylinders of the same length and same gap width, six pairs of equidistant vortices appear for quasi-steady acceleration, while for higher rates of acceleration the number is seven or eight, as was demonstrated by Wimmer (1988). The regimes of existence of the various configurations occurring between conical cylinders, and their changes from one mode into another, will be described later during the discussion of the effect of different gap sizes in §8.

5.2. *Unsteady states*

Between rotating conical surfaces another vortical flow exists, which is unsteady for all supercritical Reynolds numbers. The vortices are no longer closed toroidal cells with azimuthal axes, but inclined to the horizontal plane. They are no longer travelling upwards, but downwards. An unsteady flow with helical vortices is observed, as illustrated in figure 9. The vortices wind around the inner cone like a coil and the whole system of vortices moves downwards.

This axial downward propagation of the helical vortices is caused by two different effects: firstly, by a rotation of the helix itself, and secondly by compensation for the mass transport in such a helical vortex tube.

Upon rotating a solid helix, an observer in a stationary system has the impression of an axial movement of the helix. Depending on whether it is a right- or a left-hand helix, or whether it rotates clock- or counterclockwise, an axial motion is observed that is directed up- or downwards. In the present case a right-hand helix with a clockwise rotation, or a left-hand helix with a counterclockwise rotation of the inner cone always produces a downward motion. For the same arrangement, the compensation for the

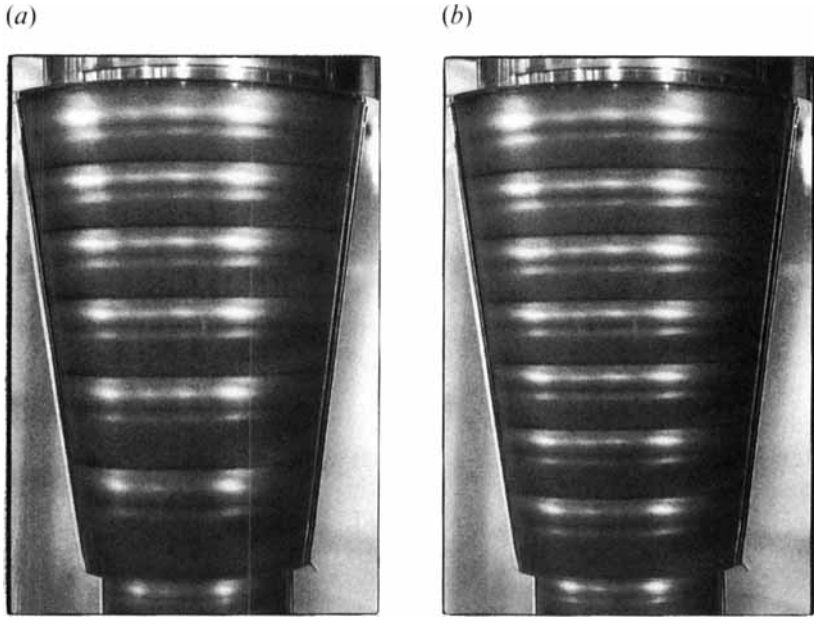

FIGURE 8. Flow configurations for different initial acceleration rates; (*a*) six pairs of vortices, $Re = 1543$; (*b*) seven pairs of vortices, $Re = 2098$, $s = 10$ mm.

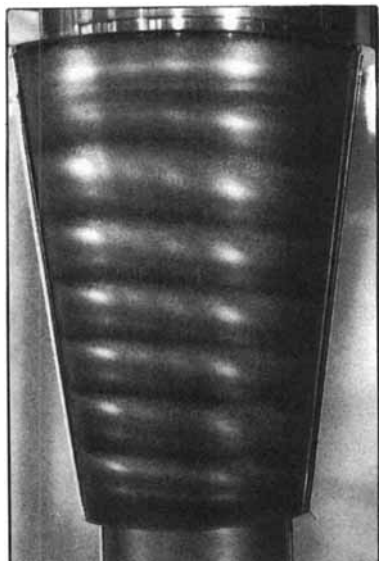

FIGURE 9. Unsteady helical vortices, $s = 10$ mm, $Re = 950$.

mass transport causes the same downward motion. It is therefore necessary to examine whether the helical vortex system rotates at all and if it does, to determine the rate of rotation.

This was done by using a stroboscope adjusted to the same frequency as the rotating helix, so that the helical vortex system seems to be fixed in the azimuthal direction. For very low angular velocities the rotation rate was determined by counting the rounds per minute, thus giving a high accuracy in the lower velocity regimes. In the measurements,

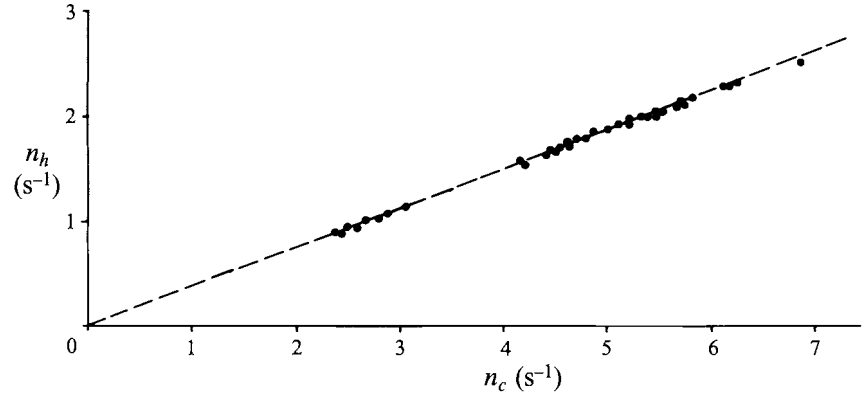

FIGURE 10. Ratio of the angular velocity of the rotating cone and the helix.

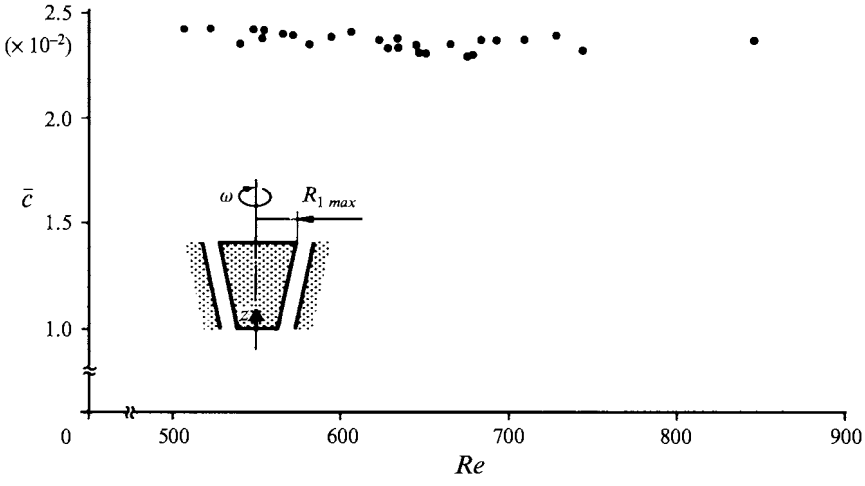

FIGURE 11. Velocity $\bar{c} = c/R_{1max}\omega$ of the helical vortices; c is the actual measured velocity, $Re = R_{1max}^2\omega/\nu$.

shown in figure 10, a fixed ratio between the rotation of the cone n_c and the rotation of the helix n_h was found. In the investigated range, this ratio is $n_h/n_c = 0.38$, with an accuracy between 2% and 3%.

The second effect of the downward propagation is based on compensation for the mass transport. In every vortex tube, and in a helical vortex also, mass transport takes place. Since in the present case the inclination of the helix is upwards, viewed in the flow's direction, the fluid is also transported this way. In a closed system, as described here, the mass transport must somehow be compensated for. This happens such that the entire helical system moves downwards with a velocity depending on the amount of fluid conveyed. The mass transport in turn depends on the angular velocity of the rotating cone. The velocity of the downwards propagating helical vortices was measured in the same way as described for the upwards travelling toroidal vortices. Figure 11 shows the downward velocity of the helical vortices, caused by the helix rotation and mass transport compensation; the major part is due to the helix rotation. As is evident from figure 11, the dimensionless velocity remains nearly constant over a wide range of Reynolds numbers. It seems, however, that there is a slight decrease at higher Reynolds numbers; this effect was confirmed by a number of measurements.

In the literature there are many references to moving helical vortices. They occur preferentially in the annulus between counter-rotating cylinders. Coles (1965) described the occurrence of helical vortices in an annulus between two cylinders as 'a spiral band, either right- or left-hand, which rotates steadily at mean angular velocity without changing its shape or losing its identity'. Andereck, Liu & Swinney (1986) reported two different systems of helical vortices with opposite inclinations, existing simultaneously side by side. For such an arrangement, both helical systems must move in opposite directions as was observed during their experiments. Moreover, from the direction of inclination and movement of the vortices, the sense of the inner cylinder's rotation can be deduced.

Systems of moving helical vortices have also been mentioned by P. S. Marcus (1993, personal communication) for counter-rotating cylinders before turbulent 'bursts' occurred, as well as by I. Mutabazi (1993, personal communication) for horizontally counter-rotating cylinders, only partly filled with a fluid. Both detected moving 'spirals' or 'inclined travelling rolls', the behaviour of which is in accordance with the considerations mentioned above.

Taylor's (1923) observations of 'spiral' vortices, however, are not directly comparable with these phenomena, since he reported 'that one of the vortices was unusually wider than the other', while the 'spiral' configuration of Coles, Andereck *et al.* and others relates to vortices of equal size.

In the case of conical cylinders, the angle of inclination of the helical vortices changes over the axial length. The change is necessary because of the varying cross-section of the annulus. The different extension of the vortices with the local axial position causes a variation of the cross-section of such a vortex tube and is followed by a change in the local mass transport. Since the overall mass transport must be constant, the angle of inclination is altered as a consequence. Hence, different independent factors make it very difficult to determine the angle of the helical vortices.

To prove that the helix is single, we arranged two mirrors obliquely behind the cones so that the rear and both sides of the cone are visible, and an image of the entire circumference is obtained together with the front view. It is then possible to see the whole vortex tube completely and to confirm that the helix is single.

The downwards moving helical vortices may be generated by a disturbance which is not rotationally symmetric, and is not damped but excited by an increased angular velocity. This behaviour depends on the rate of acceleration, and is very similar to a corresponding flow mode between cone–cylinder combinations, previously described by Wimmer (1992).

5.3. *Combinations of final steady and unsteady states*

Since the occurrence of unsteady helical vortices also depends on initial conditions, it is possible to generate different configurations. Of special interest is the existence of a combination of steady and unsteady vortex flows in the annulus. This happens such that the steady toroidal vortices occupy one part of the annulus, the upper or the lower, and the unsteady helical vortices the other part. Such a configuration is shown in figure 12(*a*). Likewise, it is possible, again depending on initial accelerations, that helical downwards moving vortices are confined between steady toroidal ones, as may be seen in figure 12(*b*). In this figure, there appears to be a larger number of toroidal cells in the upper than in the lower part. The opposite case is also experimentally detectable. Hence, between rotating conical surfaces there is the rare case of unstable steady and unsteady flows co-existing. This presents a challenge to mathematicians studying branching processes in fluid mechanics.

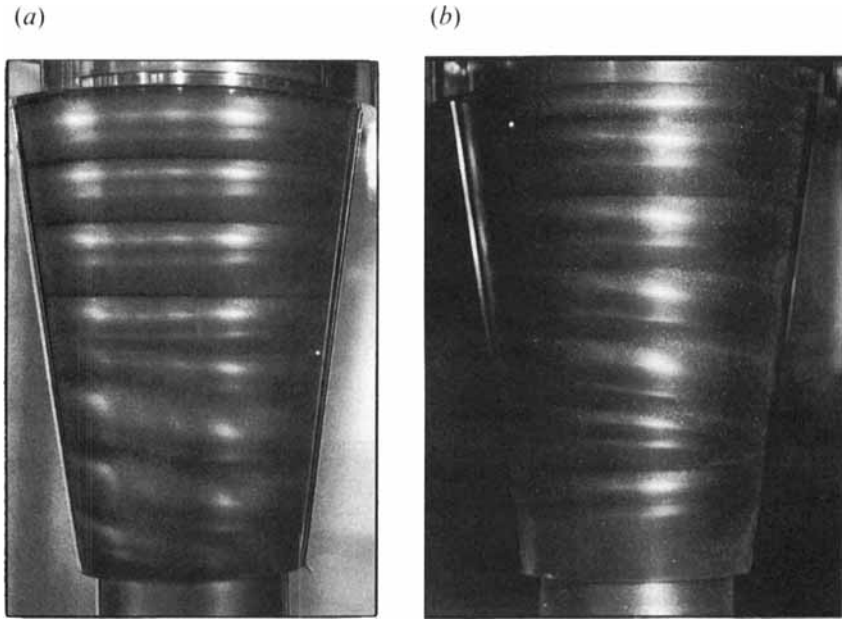

FIGURE 12. Combinations: (*a*) toroidal vortices occurring above helical vortices, $Re = 1116$; (*b*) unsteady helical vortices between steady toroidal vortices, $Re = 1811$, $s = 10$ mm.

6. Wavelength of vortices

The wavelength of the pattern is an important measure for the characterization of an unstable flow. Normally the wavelength λ of such a flow is determined by the length of a vortex pair. Since in the present case nearly every vortex is different from every other, only the extension of a single vortex cell $\bar{\lambda}$ is used to define the wavelength. This length is made dimensionless by the gap size s to give $\lambda' = \bar{\lambda}/s$.

The influence of the meridional flow leads to the alternately large and small cells in the annulus mentioned earlier. As is evident from figure 7(*b*), even the large and small vortices have different extensions for different local axial positions. A 'large' vortex at the bottom is greater than a 'large' one at the top because of the interaction of the locally different strength of the vortex cells and meridional flow mentioned above. Vigorous vortices in the upper part are less stretched by the weaker meridional flow than those in the lower part, and vice versa. The 'wavelength' λ' of a vortex cell not only depends on its sense of rotation, but also on its local axial position.

Results of wavelength measurements are shown in figure 13. The dimensionless 'wavelength' λ' for co-rotating and contra-rotating vortices is plotted separately versus the dimensionless axial length of the cone for Reynolds numbers of $Re = 1535$ and 2065. It may be noted that vortices rotating in the direction of the meridional swirl are clearly larger than those rotating opposite to it. Contra-rotating vortices have an axial length approximately equal to the gap width, as can be seen in figure 13. For co-rotating vortices, the dependence on the axial position is clearly discernible. The decrease of the 'wavelength' of these vortices along the axis is obvious, ranging from 2.3 times the gap width to about the gap size, depending on whether they are near the top or the bottom. The influence of the Reynolds number is negligible.

A similar independence from the Reynolds number is also observed for selected measurements of separate vortices in the middle of the annulus. Only for cells adjacent to the end plates have we noticed an influence of the Reynolds number (cf. Wimmer

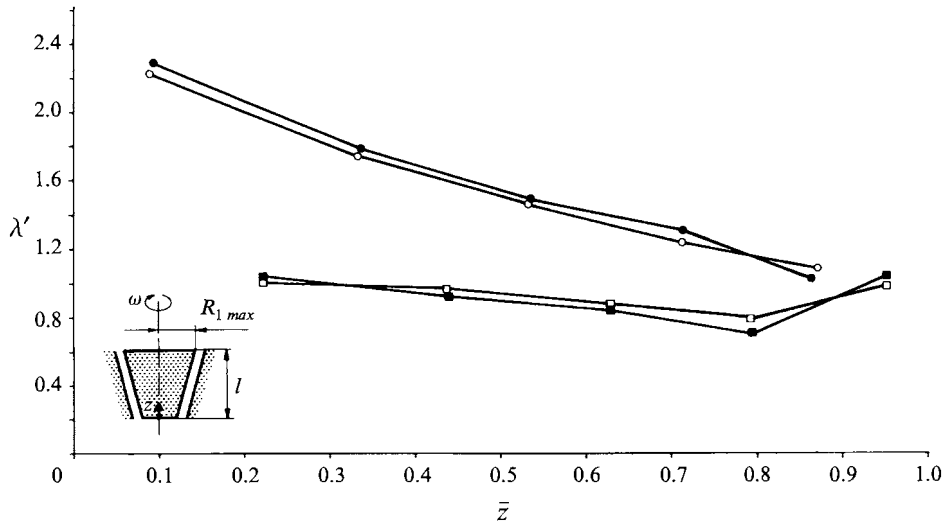

FIGURE 13. The 'wavelength' of the vortices. Mode with five vortex pairs. $\lambda' = \bar{\lambda}/s, \bar{z} = z/l$, $Re = R_{1max}^2\omega/\nu$ and $s = 10$ mm, $Re = 2065$: ●, co-rotating vortices; ■, contra-rotating vortices. $Re = 1535$; ○, co-rotating vortices; □, contra-rotating vortices.

1994). For different initial accelerations not only is a different number of cells generated with correspondingly different wavelengths, but also the further development is altered. For a larger number of cells, e.g. fourteen, the difference in size between co- and contra-rotating vortices becomes smaller compared with the case of ten cells in the annulus described above. A similar behaviour is also observed for other boundary conditions, such as rotating end plates. More detailed information on this effect may be found in Wimmer (1994).

In conclusion, we found that the 'wavelength' of vortices between coaxially rotating cones is a function of: (i) the width of the gap; (ii) initial conditions; (iii) the sense of rotation of the vortices; (iv) the local axial position of the vortices. Such a multiple dependence of the 'wavelength' on different factors is a newly discovered effect and had until now only been observed for combinations of cylinders and cones (Wimmer 1992).

7. Various boundary conditions

Having discussed the effect of different initial conditions, the influence of various boundary conditions should be described. Here, the boundary conditions are varied by end plates limiting the annulus. End plates can influence the developing flow either by their geometry or by their dynamic effects. During the experiments, end plates were applied which bridged the gap either completely or only partially, being either stationary or rotating. The following section treats solely the gap width $s = 10$ mm, since characteristic flow configurations can be demonstrated very clearly in this case.

7.1. *Stationary end plate partly bridging the gap*

If the end plate at the top bridges the gap only partly, as displayed in figure 1, another smaller annulus is formed between the rotating body and the end plate. This annular cylindrical gap is also filled with the working fluid and is involved in the flow events beneath. This results in considerable differences regarding the further development of the vortices.

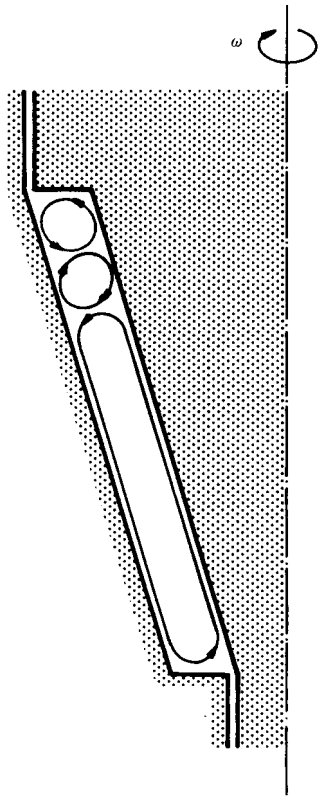

FIGURE 14. Location and sense of rotation of the first vortex that occurs for a rotating end plate.

For slightly supercritical Reynolds numbers, toroidal vortex cells again travel upwards. If the gap is only partly filled with vortices, the first clockwise rotating vortex with a radial inward flow at the top remains. The next three are compressed to form one single counterclockwise rotating vortex. The next pair follows, exactly as described before. If however, by increasing the Reynolds number, the annulus is completely filled with vortices, their behaviour changes drastically.

Now, the vortex at the top no longer remains, but is compressed, and then pushed into the smaller annular gap above. The adjacent vortices then move with a periodicity depending on the angular velocity. Hence, at a stationary half-covering end plate, alternately clockwise or counterclockwise rotating vortices occur, so that a radial outward flow can exist at a stationary end plate. In addition, the number of vortices changes periodically, since only one vortex is suppressed at the top whilst a new pair is generated at the lower end. This results in an alternating even or odd number of cells in the annulus.

These vortex patterns can be obtained not only as transient but also as final states. By applying a sudden acceleration when there is just an odd or even number of vortices in the annulus, this configuration becomes fixed, and a final state with an odd or even number of cells is established, respectively. By imposing different initial accelerations, the whole variety of vortex configurations with ten to fifteen cells can be generated for a gap width of $s = 10$ mm and a length of $l = 125$ mm, if a stationary half-covering end plate is used. The velocity of the upwards travelling vortices is analogous to that for stationary end plates bridging the gap completely, as shown in figure 6.

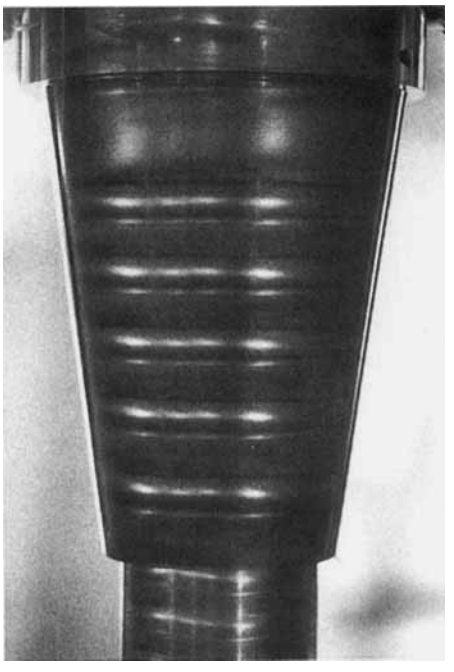

FIGURE 15. Configuration with eleven pairs of vortices for a higher rate of initial acceleration with a rotating end plate; $s = 10$ mm, $Re = 2239$.

7.2. *Rotating end plate completely bridging the gap*

The end plate at the lower end of the gap remains at rest, but the top one now rotates with the angular velocity of the inner cone. This arrangement produces asymmetric boundary conditions, resulting in an odd number of vortex cells in the annulus.

At the rotating end plate at the top, the flow is always directed outwards, independent of whether there is a sub- or supercritical flow in the gap. Increasing the Reynolds number to the critical value, a pair of vortices is formed together with the rest of the undisturbed basic flow, as sketched in figure 14. This development is different from the case with a stationary end plate, where at first one vortex with the adjacent basic flow is always observed (figure 3). For higher Reynolds numbers, further pairs of vortices are added in the direction of the smaller radius, until only a small part of the basic flow remains, forming a single vortex. Thus, a configuration is obtained with an odd number of vortices in the annulus. By applying different rates of acceleration, nine, eleven or thirteen vortices can be generated; figure 15 shows such a configuration with eleven vortices.

The 'wavelength' of the vortices in this case depends again on the gap width, acceleration rate, sense of rotation and local axial position, as was pointed out before. The same is true for the behaviour of co- and contra-rotating vortices, with respect to their axial position. However, the top vortex cell is actually larger than usual, because of the rotating end plate. This effect is clearly demonstrated by figure 15. As before, the toroidal vortices travel upwards at first. The initial and final behaviour as well as the behaviour of the upward motion is the same as that for stationary end plates.

Unsteady helical vortices are also detectable with an upper rotating end plate. Such a helical flow is, however, more difficult to produce, since the end plate's rotation strongly suppresses non-rotationally symmetric disturbances. Therefore, mostly combinations of toroidal and helical vortices appear. This preferential state is shown

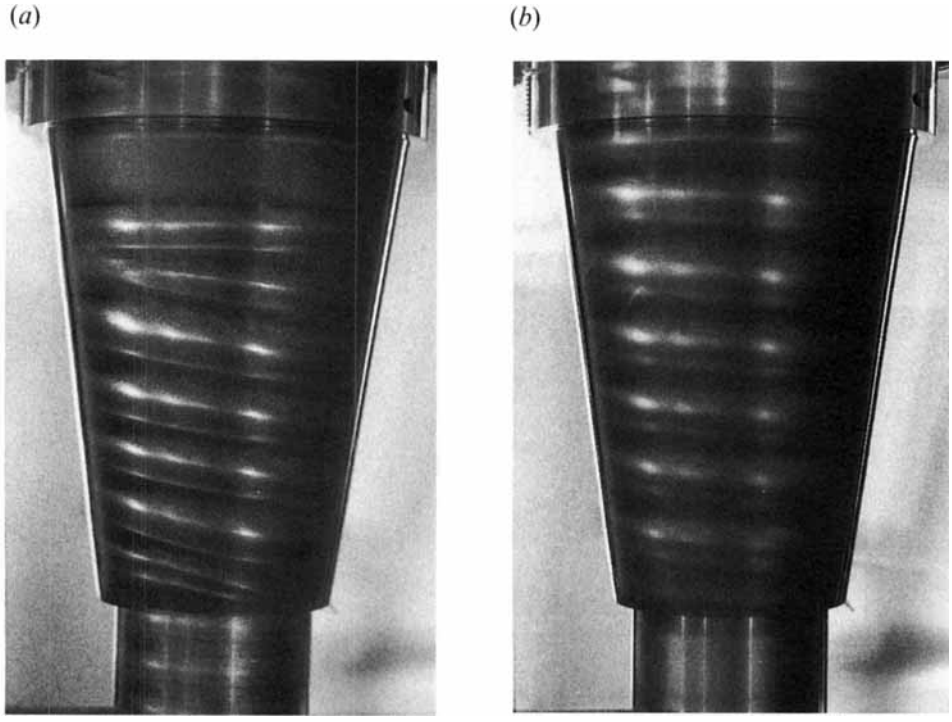

FIGURE 16. Unsteady helical vortices with a rotating end plate: (*a*) combination of toroidal and helical vortices, $Re = 1489$; (*b*) helical vortices in the whole annulus, $Re = 557$, $s = 10$ mm.

in figure 16(*a*) displaying steady toroidal vortices near the rotating end plate, where its influence is dominant, and helical ones in the lower part of the annulus. Only if a very strong acceleration is applied during the generation of the first helical vortices can these advance as far as the rotating end plate and exist as a final state. Such a rare situation is documented in figure 16(*b*). Therefore, unstable flows with helical vortices can be produced between rotating circular and conical cylinders, even with a rotating end plate, and likewise for non-constant gap geometries, as was demonstrated by Wimmer (1992) for cylinder–cone combinations.

For a rotating end plate bridging the gap only partly, the vortex at the top can no longer be pushed through the small opening between the rim of the end plate and cone, as is possible for stationary end plates. Therefore, the influence of the geometry of the end plate is suppressed by its rotation. Thus, fundamental changes and new configurations cannot be expected and have not been noticed.

8. The effect of gap size

Besides the previously discussed gap size of $s = 10$ mm, three smaller gap widths of $s = 5$, 6, 7 mm were investigated. Special effects relating to these smaller gap sizes are now described. Only the most relevant case of two stationary end plates, which bridge the gap completely, is considered.

8.1. *Gap size $s = 5$ mm*

For the smallest gap width of $s = 5$ mm, vortices appear first at the smallest Reynolds number $Re = 1123$, corresponding to the critical Taylor number $Ta = 41.6$. This number is an average from many measurements, with a relatively high tolerance band

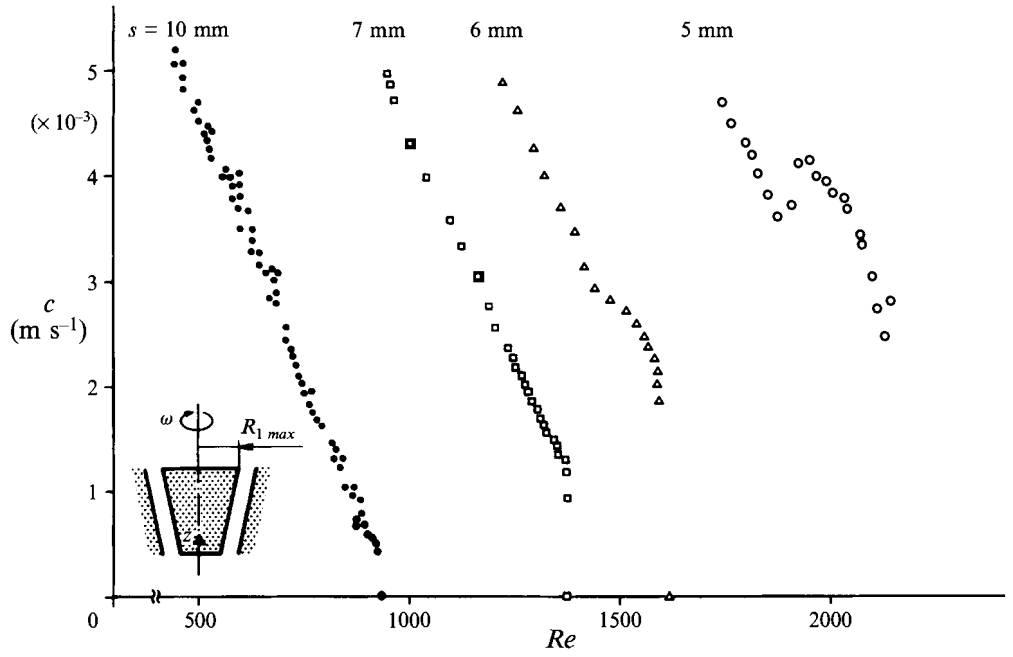

FIGURE 17. Comparison of the vertical velocity c of travelling vortices for different gap widths; c is the actual measured velocity, $Re = R_{1max}^2 \omega/\nu$.

of 5%, since the onset of the vortices is recorded solely by flow visualization. Toroidal vortices start to travel upwards at $Re = 1350$. Increasing the angular velocity, the vortices still travelling become wavy at $Re = 2012$, or at $Ta/Ta_c = 1.8$.

The velocity of the travelling vortices is greatest for the smallest gap size, as discussed in §§3 and 4. Initially the travel velocity shows the expected linear trend, as can be seen in figure 17. At higher Reynolds numbers, when the vortices become wavy, a discontinuity appears, indicating higher velocities for wavy vortex flow. A final steady state, even with wavy vortices, was not found for a gap width of $s = 5$ mm. Therefore, no regimes of existence nor measurements of the wavelength of the vortices are available for this small gap size.

As with all other investigated gap widths, downwards moving vortices can be observed. The inclination angle of the helix is measured in the lower part of the annulus as $\alpha = 3°$, in the upper part as $\alpha = 1.5°$ and in the midsection as $\alpha = 2°$. A comparison with other gap sizes show that the inclination angle increases with increasing gap width.

8.2. *Gap size s = 6 mm*

For a gap width of $s = 6$ mm, toroidal vortices start to travel upwards at $Re = 990$, and at about $Re = 1080$ the annulus is entirely filled with vortices. Wavy vortices occur at $Re = 1510$. As in the previous case, a discontinuity in the trend of the velocity of the travelling vortices, when wavy patterns appear, is seen. However, for this gap width, a steady state can be obtained for the first time at $Re = 1666$, even if only with wavy vortices. Unsteady helical vortices occur having an inclination angle of $\alpha = 3°$ in the middle section.

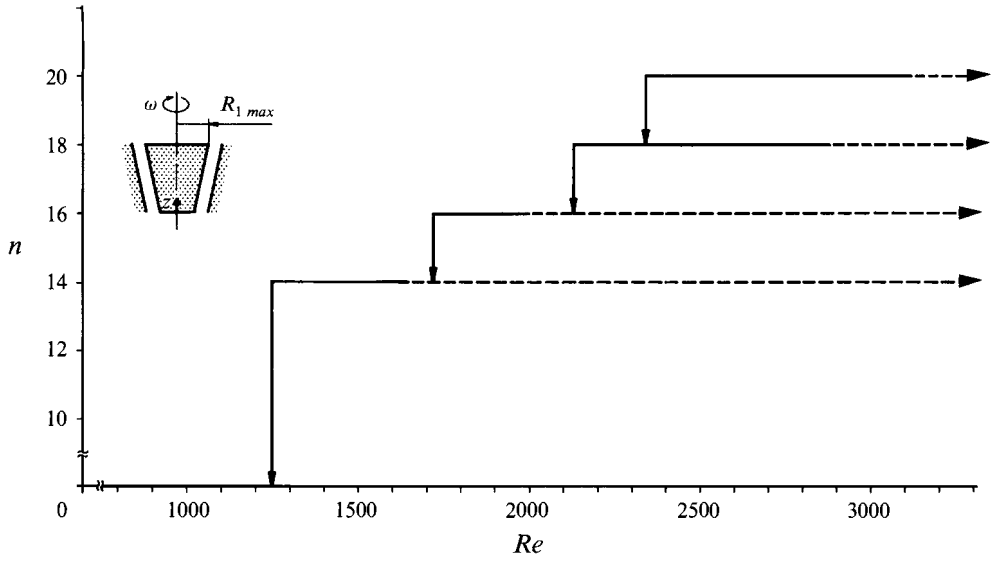

FIGURE 18. Regimes of existence for different vortex modes, $s = 7$ mm, $Re = R_{1max}^2 \omega/\nu$, n = number of vortices: ——, toroidal vortices; – – –, wavy vortices. The arrows indicate the change from one mode to another for decreasing Reynolds numbers.

8.3. *Gap size s = 7 mm*

For a gap size of $s = 7$ mm, the vortices start to travel upwards at $Re = 777$, and the annulus is entirely filled with vortices at $Re = 874$. Travelling wavy vortices have not been detected for this gap width, as is also manifested by the linear trend of the velocity of upwards moving vortices without a discontinuity, shown in figure 17. Besides this linear decrease, the jump from a just existing travel velocity to a stand still can be seen very clearly. Figure 17 also shows that this jump decreases with increasing gap width. For $s = 7$ mm, a final steady state with toroidal vortices is established at $Re = 1375$. The vortices can become wavy for higher Reynolds numbers at about $Re = 1700$, giving $Ta/Ta_c = 2.6$.

Since for $s = 7$ mm final steady states with toroidal vortices are obtained for the first time, it is possible to generate different configurations by using different rates of acceleration. With increasing acceleration rates, modes with seven, eight, nine or ten pairs of vortices may occur. Their regimes of existence are given in figure 18. This diagram shows very clearly that modes with a higher number of vortices exist at higher Reynolds numbers. Solid lines characterize modes with toroidal vortices and dashed lines those with wavy vortices. By decreasing the Reynolds number, a mode with a higher number of vortices changes to a mode with a smaller number of vortices, indicated by the arrows.

The wavelength of the vortices has also been determined and shows the same characteristics as those described in §6. It should be mentioned, however, that the largest co-rotating vortex has an extent of about 2.1 times the gap width for seven pairs of vortices while this value is only 1.7 for a configuration with ten pairs of vortices in the annulus. Helical vortices are moving downwards as before. The inclination angle is again greater at $\alpha = 3.5°$ in a middle axial position. The change of the inclination angle with the cone's length is shown in figure 19. The angle of the helical vortices is relatively constant in the midsection of the cone, but increases towards the bottom of the cone and decreases towards its top. Such behaviour is typical for all investigated

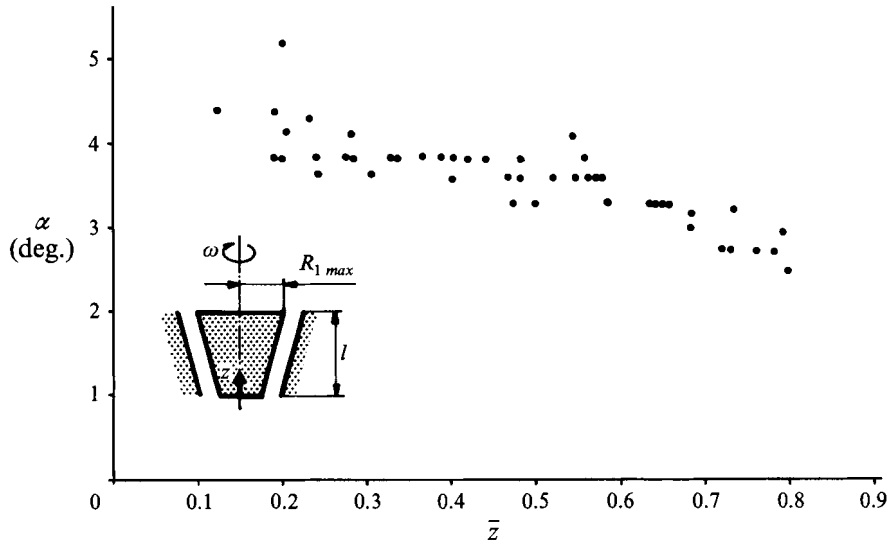

FIGURE 19. Inclination angle of helical vortices as function of the local axial position, $\bar{z} = z/l$.

gap sizes. These values of the inclination angle increase, however, with increasing gap width.

8.4. *Gap size s = 10 mm*

Since the development and behaviour of the flow between rotating cones described in previous sections have been exemplified in terms of the 10 mm gap size, only very special features are now mentioned. The first vortex appears at the top end of the annulus at $Re = 373$, corresponding to $Ta = 46.7$, which is in good accordance with Kirchgässner's (1961) theory. Toroidal vortices start to travel upwards at $Re = 455$, and at $Re = 544$ the annulus is entirely filled with vortices. Finally, at $Re = 930$, the steady state is established. The different final configurations have been explained before. In contrast to the 7 mm gap size, there are only three modes of flow with five, six or seven vortex pairs. Their regime of existence, as well as their changes into other modes with decreasing Reynolds numbers, are illustrated in figure 20. It should be emphasized that no regular wavy vortices are detectable for $s = 10$ mm. The angle of unsteady helical vortices is about 4° in a mid-axial position.

8.5. *Comparison*

For all gap sizes, the first Taylor vortices appear at the largest radius. Upon increasing the Taylor number, more vortices are added in the direction of the smaller radius and later they travel upwards as closed toroidal cells. The velocity of the travelling vortices is however different for different gap sizes. For a constant Reynolds number, the velocity is higher for a smaller gap width, as exhibited in figure 17, which shows dimensional velocities for all gap sizes. The linear decrease of the travel velocity with increasing Reynolds number is apparent and is valid for all gap sizes, as long as no wavy vortices appear. Their occurrence is marked by a discontinuity in the curves, as for $s = 5$ and 6 mm. For larger gap sizes, above $s = 7$ mm, a final steady state with toroidal vortices is possible, but for smaller gap sizes, this is only possible with wavy vortices, if at all. If a steady state exists, various vortex configurations are observable, generated either by different initial accelerations or by a change from one mode to another.

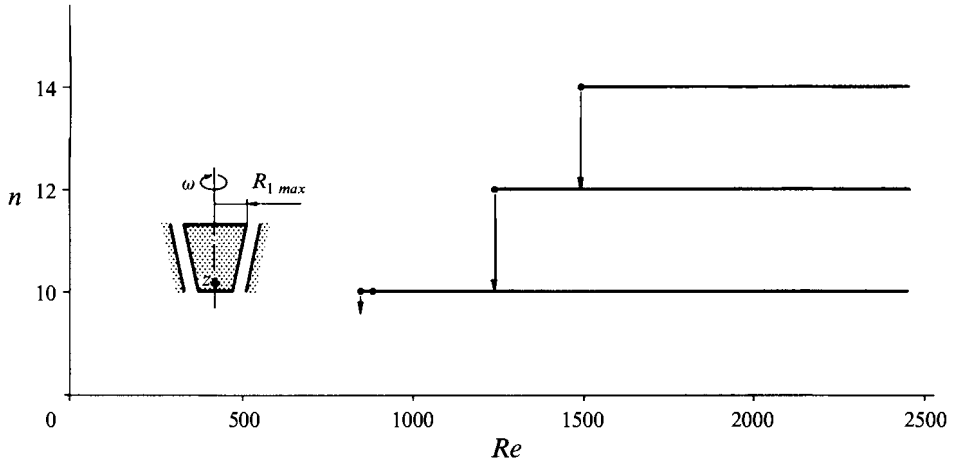

FIGURE 20. Regimes of existence for different vortex modes, $s = 10$ mm, $Re = R_{1max}^2 \omega/\nu$, n = number of vortices. The arrows indicate the change from one mode to another for decreasing Reynolds numbers.

The 'wavelengths' of the vortices are only comparable for larger gap sizes for which steady states exist. Then the following rule holds: vortex cells in a middle section of the annulus, rotating in the direction of the meridional swirl are always larger than adjacent vortices rotating opposite to the meridional velocity. Furthermore, for quasi-steady accelerations, co-rotating vortices are always larger than the corresponding gap size. The difference in the size of co- and contra-rotating vortex cells is more pronounced the larger the gap width and the smaller the number of vortices in the annulus is.

A higher number of vortices in the annulus is obtained for smaller gap sizes and for higher rates of acceleration. Regimes of existence of the different modes are shifted to smaller Reynolds numbers with increasing gap widths. For all investigated gap sizes, a configuration with unsteady helical vortices occurs consisting of a single helix, with its downward movement mainly dependent on the angular velocity. The inclination angle of the helix is larger in the lower section of the annulus than in the upper, and increases with increasing gap width.

9. Conclusions

The present research demonstrates that a relatively small geometrical change in the conventional Taylor–Couette apparatus has far-reaching consequences for the onset and the behaviour of Taylor vortices. The rotating cones cause a three-dimensional basic flow which has a crucial influence on the resultant vortices. By applying different initial and boundary conditions, a wide variety of vortex configurations is possible in an annulus between conical surfaces.

Owing to different centrifugal forces over the cone's length, sub- and supercritical regions may co-exist, so that undisturbed basic flow and Taylor vortices occur side by side in a conical annulus. Over a wide range of Reynolds numbers, the vortices are unsteady. A most important result is, therefore, that a system of toroidal vortices can travel through a closed flow system, without any external influence.

The velocity of upwards travelling vortices decreases with increasing gap widths for constant Reynolds numbers. In other words, for the same velocity of travel, smaller

Reynolds numbers are necessary for larger gap sizes. For the same reason, a steady final state cannot be established for smaller gap widths, or, if at all, only in the form of wavy vortices. Furthermore, different end plates seem to have no influence on the velocity of upwards travelling vortices.

The basic flow as well as the rotation of the vortices change along the axis of the cone. The interaction of the locally different vigour of the basic flow and the vortex flow causes major effects. Depending on the ratio between the basic flow and the vortex flow, the whole system of vortices is either shifted, i.e. it travels, or the influence of this flow ratio is confined to single vortex cells, resulting in their deformation. The interaction of the locally different basic flow and vortex flow also causes the new effect of a dependence of the 'wavelength' on multiple parameters.

The downward movement of unsteady helical vortices can be explained by a rotation of the helix and by a compensation of the mass transport. The inclination angle of the single helix varies over the cone's length. It increases, however, with the gap size.

It is also interesting and a rare case in fluid dynamics that a combination of stationary toroidal and moving helical vortices can occur simultaneously, so that unstable steady and unsteady flows co-exist. In general, the wide variety of possible vortex patterns is a most fascinating occurrence in the gap between rotating cones.

The dynamical behaviour of the various vortex configurations shows interesting relations to other thermal and hydrodynamical systems, as was demonstrated by Bühler, Schöder & Wimmer (1994). Hence, the investigation of the flow between rotating conical surfaces is of fundamental interest for basic fluid mechanics. Its study can contribute to a better understanding of pattern-building systems.

The author thanks Bernhard Denne, who studied, for his semester thesis, the smaller gap sizes from $s = 5$ to 7 mm. I would also like to thank J. E. R. Coney for his help with the preparation of this manuscript.

REFERENCES

ABBOUD, M. 1988 Ein Beitrag zur theoretischen Untersuchung von Taylor Wirbeln im Spalt zwischen Zylinder/Kegel Konfigurationen. *Z. Angew. Math. Mech.* **68**, 275–277.

ANDERECK, C. D., LIU, S. S. & SWINNEY, H. L. 1986 Flow regimes in a circular Couette system with independently rotating cylinders. *J. Fluid Mech.* **164**, 155–183.

BÜHLER, K., SCHRÖDER, E. & WIMMER, M. 1994 Dynamics of flow instabilities in thermal and hydrodynamic systems. *Acta Mechanica* Suppl. 4, 1–9.

BURKHALTER, J. E. & KOSCHMIEDER, E. L. 1973 Steady supercritical Taylor vortex flow. *J. Fluid Mech.* **58**, 547–560.

BURKHALTER, J. E. & KOSCHMIEDER, E. L. 1974 Steady supercritical Taylor vortices after sudden starts. *Phys. Fluids* **17**, 1929–1935.

COLES, D. 1965 Transition in circular Couette flow, *J. Fluid Mech.* **21**, 385–425.

DONNELLY, R. J. 1992 Evolution of instrumentation for Taylor–Couette flow. In *Ordered and Turbulent Patterns in Taylor–Couette Flow* (ed. C. D. Andereck & F. Hayot), pp. 1–27. Plenum.

KIRCHGÄSSNER, K. 1961 Die Stabilität der Strömung zwischen rotierenden Zylindern gegenüber Taylor–Wirbeln für beliebige Spaltweiten. *Z. Angew. Math. Phys.* **12**, 14–30.

TAYLOR, G. I. 1923 Stability of a viscous liquid contained between two rotating cylinders. *Phil. Trans. R. Soc. Lond.* A **223**, 289–343.

WIMMER, M. 1976 Experiments on a viscous fluid flow between concentric rotating spheres. *J. Fluid Mech.* **78**, 317–335.

WIMMER, M. 1983 Die viskose Strömung zwischen rotierenden Kegelflächen. *Z. Angew. Math. Mech.* **63**, 299–301.

WIMMER, M. 1988 Viscous flows and instabilities near rotating bodies. *Prog. Aerospace Sci.* **25**, 43–103.

WIMMER, M. 1992 Wirbelbehaftete Strömung im Spalt zwischen Zylinder–Kegel Kombinationen. *Rep.* 45, pp. 59–83. Strömungsmechanik und Strömungsmaschinen, Universität Karlsruhe.

WIMMER, M. 1994 Strömungen im konstanten Spalt zwischen rotierenden Kegelflächen. *Rep.* 47, pp. 13–42. Strömungsmechanik und Strömungsmaschinen, Universität Karlsruhe.